J. Astrophys. Astr. (1990) **11**, 221–235

A Search for Protocliisters at z = 3.3

Ravi Subrahmanyan *Radio Astronomy Centre, Tata Institute of Fundamental Research, Post Box 8, Ootacamund 643001*

K. R. Anantharamaiah *Raman Research Institute, Bangalore 560080*

Received 1989 December 13; accepted 1990 April 17

Abstract. We have used the Very Large Array to image a single field in a set of adjacent frequency bands around 333.0 MHz in an attempt to detect 21 cm emission from large scale H I inhomogeneities at a redshift of $z = 3.3$. Following the subtraction of continuum radio sources, the absence of any spectral signals apart from that expected due to the system thermal noise has been used to derive constraints on the evolutionary scenario leading to the formation of the present day clusters of galaxies. The observations rule out the existence of H I protoclusters at $z = 3.3$ with masses $\simeq 3.5 \times 10^{14}\ M_{\odot}$ in H I gas and space density exceeding $(74\ \mathrm{Mpc})^{-3}$. This indicates that the present day rich clusters of galaxies either formed as gaseous protocluster condensates prior to $z = 3.3$ or else they formed through the clustering of their constituent galaxies.

Key words.: Clusters of galaxies, formation—HI observations—HI regions, cosmological—protoclusters

1. Introduction

Structure in the Universe on large scales is believed to have formed by the growth of seed density perturbations through gravitational instabilities (Peebles 1980). In theoretical scenarios where short wavelength fluctuations are damped as a consequence of astrophysical processes like the Silk (Silk 1968; Peebles & Yu 1970) or Landau (Bond & Szalay 1983) damping mechanisms, the first objects that condense out of the Hubble flow are expected to have scales exceeding clusters of galaxies. During the epoch corresponding to a redshift of z when these protoclusters are predominantly neutral gaseous condensates, the 21 cm emission from neutral hydrogen atoms in the matter inhomogeneities is expected to be observable around a frequency of $1420.4/(1 + z)$ MHz. The observational consequences have been discussed by Sunyaev & Zel'dovich (1974), Hogan & Rees (1979) and more recently by Subrahmanyan (1990) for a variety of plausible evolutionary scenarios.

Several observational attempts have been made to detect this 21 cm emission from cosmological redshifts. Each such experiment has searched an area of the sky over an observing bandwidth. The noise levels, in units of .flux density, vary in the different searches and also take on a range of values depending on the spatial and spectral resolution in the observational data. The relationship between these search parameters and physical quantities in the emitter's frame is determined by the Cosmology.

The search volume, located at a redshift determined by the observing frequency, has a line-of-sight depth determined by the bandwidth, and a face area determined by the sky area covered. Condensates having a specific line-of-sight velocity dispersion are optimally detected by data having the corresponding frequency resolution, with upper limits on the observed flux density yielding upper limits on the H I masses of these condensates.

Constraints on the existence of supercluster mass condensates require searches covering large volumes since these objects have small space densities. But these searches can be performed with relatively low sensitivity because the superclusters have large masses. Useful observational constraints on the existence of proto-superclusters have been placed at both z = 3.3 (Subrahmanyan & Swarup 1990) and at z = 8.4 (Bebbington 1986). In this paper we are concerned with observations that constrain the existence of lower mass protoclusters, the progenitors of the present day clusters of galaxies, whose detection requires searches with relatively higher sensitivity, but where smaller search volumes suffice. A preliminary search for protoclusters using the Very Large Array was reported by Hardy & Noreau (1987). A protocluster search using the Westerbork Synthesis Radio Telescope (WSRT) was conducted by de Bruyn *et al.* (1988).

As a complementary experiment to the Ooty search for proto-superclusters (Subrahmanyan & Swarup 1990), we have conducted sensitive observations using the NRAO Very Large Array (VLA; Thompson *et al.* 1980; Napier *et al.* 1983) in an attempt to detect protoclusters or any signatures of inhomogeneous H I at z = 3.3. In contrast with the Ooty observations, the VLA search had better resolution and sensitivity in order to detect the lower mass protoclusters. Since these objects of smaller mass are expected to be more abundant, the volume surveyed was also correspondingly reduced. Although our sensitivity is not an improvement on the WSRT effort (de Bruyn *et al* 1988), the volumes surveyed are independent and our interpretations of the observational data differ in methodology and viewpoint. The Hubble constant H_0 = 75 km s^{-1} Mpc^{-1}, and a density parameter Ω_0 = 1 corresponding to an Einstein-de Sitter universe, are used in this paper. Regions of Universe situated at the redshift of z = 3.3, possessing comoving dimensions d_p Mpc along the line-of-sight and d_t Mpc perpendicular to the line-of-sight, and having zero peculiar motions, will have their emission confined to an angular size

$$\Delta\theta = 0.81\, d_t \text{ arcmin} \tag{1}$$

and a frequency range

$$\Delta\nu_0^{\mathrm{H}} = 0.17 d_p \text{ MHz}. \tag{2}$$

Structures that have a characteristic mass scale M will possess a characteristic angular scale

$$\Delta\theta = 7.07(M/10^{14}\, M_\odot)^{1/3} \text{ arcmin}, \tag{3}$$

and a characteristic frequency scale

$$\Delta\nu_0^{\mathrm{H}} = 1.46(M/10^{14}\, M_\odot)^{1/3} \text{ MHz}. \tag{4}$$

These equations relate comoving volumes and closure density masses in physical space at z = 3.3 with parameters in the observed spectral-line cube and follow from the equations presented in Subrahmanyan (1990). An optically thin gas cloud at z

= 3.3, having an H I mass $M_{H\,I}$, will be observed in its redshifted 21 cm emission with a peak flux density

$$S_p = 6.4\,(M_{H\,I}/10^{14}\,M_\odot)\,(\Delta\nu_0/1\ \mathrm{MHz})^{-1}\ \mathrm{mJy}. \quad (5)$$

2. The observations and data reduction

The observed field lies within the 5C7-survey region (Pearson & Kus 1978) and is centred at a right ascension of $08^h\ 13^m$ and a declination of + 25°00′ (coordinates are referred to 1950.0 epoch). The half-power area of the antenna primary beam contains two sources that have a flux density ~ 600–700 mJy at 333 MHz. All the other sources are ⩽300 mJy. On the average, extrapolation of the 408 MHz source counts of Pearson (1975) with an assumed spectral index of α = 0.7 (defining $S_\nu \sim \nu^{-\alpha}$) indicates that a field of this size is expected to have ~ 2 sources with flux density > 1 Jy and ~ 9 sources with flux density > 300 mJy. The total continuum flux density of all the discrete sources in the field is ~ 6 Jy, whereas the expected value is 17.1 Jy. The relative paucity of strong background continuum sources favoured the choice of this field.

The observations with the VLA were made during the night of 1986 December 22/23, from 2130 to 0730 Mountain Time (local time at the telescope site). A total of 14 antennas were used in the C configuration. The antenna primary beam has a half power beam width (HPBW) of 156 arcmin at the observing frequency, the synthesized beam has a HPBW of ~ 1 arcmin with naturally weighted visibilities, and structures of up to ~ 18 arcmin are 'visible' to the telescope in this configuration. A total bandwidth of 3.076 MHz was covered by 63 frequency channels, each of 48.828 kHz width. Channel 32 was centred at 333.00 MHz. Owing to interference being generated at multiples of 100 kHz by the electronics at the antennas, half the spectral channel data were affected by interference and consequently considerable amount of careful data rejection had to be performed by examining the visibility amplitudes as a function of time and baseline. The data were calibrated in amplitude and phase using the source 3C 196 whose flux density was calibrated using 3C 286; the flux density of this primary calibrator (3C 286) was adopted to be 26.77 Jy. Bandpass calibration was performed using the spectral response on 3C 196.

The continuum source flux density was substracted in two stages. The data in Channel 0 (an average of the data in frequency channels lying in the central three quarters of the band) were used to obtain a deconvolved image covering the half power area of the telescope primary beam. The deconvolution, using the algorithm of Clark (1980), yielded 1000 clean components containing a total of 6.255 Jy which accounts for most of the continuum flux density of the discrete sources in the image. The visibilities corresponding to these clean components were subtracted from the ungridded visibility data of all the channels. This stage of subtraction ensured that the stronger sources along with their sidelobe structure (which is frequency dependent) would be absent in later images. Each of the 63 frequency channels were then processed separately—the channel visibilities were gridded with natural weighting and without the application of any taper in order to maximize sensitivity, and the gridded data were Fourier transformed to produce images over a field of 2°.84 × 2°.84. The synthesised beam had half-power dimensions of 70 × 57 arcsec^2 and an orientation at a position angle of 75°.4. A subset of 30 channels that had relatively low

interference levels was chosen and an average image of these 'good' channel-images was subtracted from all the 63 channel-images. This second stage of subtraction removed the weaker continuum emission.

Eight channel-images suffered from the effects of severe interference and roughly half of the remaining 55 channel-images showed the effects of weaker levels of interference. The interference manifested itself as prominent east-west oriented bands over the entire image. The 55 channel-images had an average rms noise of 9.3 mJy/beam. The expected thermal noise is ~ 6 mJy/beam based on the best operational parameters of the VLA. An increase in the noise towards the edges of the passband was observed which is indicative of a decrease in the signal-to-noise ratio in the peripheral channels. This probably arises as a consequence of delay errors in the channels close to the passband edges where the antenna receiver electronics is expected to have large phase gradients.

In order to detect the interference present in the visibility data, the Fourier transform of all the channel-images were examined. The Fourier transform of an image having moderate interference essentially showed noisy data that were confined to specific tracks on the (u, v)–plane corresponding to the locations at which visibility measurements were made. A few abnormally high amplitude values were present on these tracks with a distribution over the entire range of v but mostly confined to $u \leqslant 60\lambda$ corresponding to cells in the (u, v)plane containing measurements strongly affected by interference (Thompson 1982). We rejected the effects of interference in this Fourier transform domain by setting both the real and imaginary components in these cells to zero. The inverse Fourier transform of the resulting Hermitian-form gridded visibilities returned our real celestial image, but without the east-west interference stripes. Cells in the (u, v) –plane that are blanked lie within $u \leqslant 60\lambda$ and, in addition, only the abnormally high amplitude cells have been rejected leaving other neighbouring cells unaltered. This implies that the data rejection will have a marginal effect confined to structures with angular sizes $\geqslant 30$ arcmin. Our interests are on scales $\leqslant 10$ arcmin. We find that in the data rejection for channel 32, which is a typical case, the number of (u, v)-plane cells blanked constitutes ~ 1 % of the total number of cells in the (u, v)-plane that contain visibility measurements. In order to assess the change in the 'dirty' beam due to this blanking, we made a Fourier transform of the beam corresponding to channel 32, blanked out the very same (u, v)-plane cells that were blanked in the interference rejection for channel 32, and performed an inverse Fourier transform to obtain the new beam corresponding to the interference-free image. The beam maximum was found to have reduced by 2 per cent. Owing to the use of the natural weighting scheme, cells in the central region of the (u, v)-plane have relatively higher weights. Therefore a 1 % blanking of cells in this area has resulted in the 2 per cent reduction of the beam maximum. The half power contour of the new beam differs by < 1 per cent in comparison with the original beam, which implies that subsequent to interference rejection in this manner, we do not expect the variations in the beam sizes from channel-to-channel to exceed 1 per cent. These arguments suggest that this procedure for the removal of interference stripes from the images is acceptable and hence it was followed to eliminate the effects of interference from all the affected channels. Subsequently, the channel-images have a mean rms noise of 8.8 mJy/beam.

The two stages of continuum subtraction removes all of the continuum emission that is constant across the frequency channels. Consequently, the spectral-line cube

thereafter contains only channel-to-channel relative intensities and does not contain information regarding the mean intensity at any pixel. But continuum source emission that appears in a frequency dependent form will remain. Discrete sources having spectral indicies $\alpha \sim 2.0$ (defining $S_\nu \sim \nu^{-\alpha}$) and a flux density $S_{333} \approx$ 600 mJy could leave residuals of ~ 3 mJy in the spectral line cube even after the continuum subtraction. In addition, chance superpositions of residual sidelobe responses of sources in the field-of-view can result in low order baselines. These considerations have led us to subtract linear baselines from each image pixel position. The baselines were computed by fits to the 'good' set of central 40 channels consisting of channels 13 through 53, but subtraction of the baseline was performed from all the 63 channels. Subsequently, the channel images had a mean rms-noise of 8.1 mJy/beam. The contiguous set of 41 channel-images from channel number 13 to 53, spanning a frequency range of 2.0 MHz, is free of interference and had a mean rms noise of 6.5 mJy/beam. The individual channel-images displayed rms noise values ranging from 5.6 to 8.0 mJy/beam. The rms noise in the channel-images at this final stage are plotted in Fig. 1 as a function of channel number.

3. Data analysis

The spectral signature of redshifted 21 cm emission/absorption can have a great diversity in form depending on the nature of H I distribution at the search redshift (Subrahmanyan 1990). The observed spectral-line data cube is a three dimensional

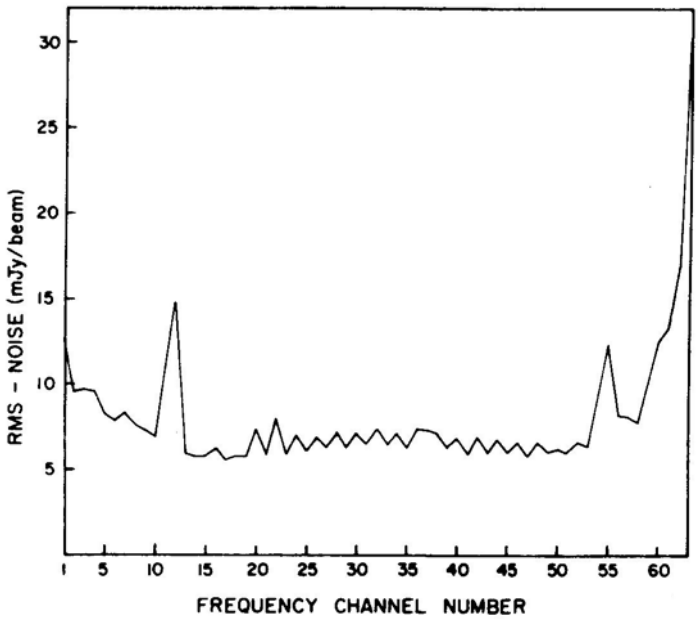

Figure 1. The rms noise in the channel-images plotted as a function of frequency channel number. These values were obtained subsequent to continuum subtraction, interference rejection and the removal of linear baselines.

array of intensities, two of the dimensions are sky coordinates (right ascension and declination) while the third dimension is the observing frequency (refer to Roelfsema 1988 for details). In the frame of the emitter at $z = 3.3$, the sky coordinate axes represent orthogonal distance coordinates perpendicular to the line-of-sight of the observer. The frequency axis denotes distance in redshift space and smearing of emission can occur along this axis if the emitting atoms have peculiar velocities with respect to the Hubble expansion. We first analyse the spectral-line cube in a model independent manner, seeking to detect signals that represent significant departures from the instrument thermal noise for different resolutions. We have smoothed the spectral-line cube to obtain four cubes, each of which have identical resolutions in all the three dimensions in comoving coordinates. We created the first smoothed cube, referred to as Cube A, by averaging channels 1 through 60 into 12 images of 5 channels each and then convolving the images to a final resolution of 70.6×70.6 arcsec^2. The resulting cube has a spatial resolution of 1.42 Mpc in all the three dimensions in comoving coordinates at $z = 3.3$. The mean matter density in the cube is expected to be $4.6 \times 10^{11}\ M_\odot$ per resolution element (assuming closure density). Using the images of channels 1 to 60, we constructed two more data cubes, referred to as Cubes B and C, having comoving resolutions of 2.84 Mpc and 4.25 Mpc. A fourth cube, D, was constructed from channels 13 through 52 by averaging 20 channels and smoothing to an angular resolution of 282.5 arcsec. A summary of the resolutions as well as the mean mass expected per resolution element for all the four smoothed cubes is contained in Table 1. The thermal rms fluctuations expected from beam-to-beam in the images of the four cubes is listed in the last column of Table 1. This noise has been estimated by considering the decrease in rms noise as a result of channel averaging and the increase due to smoothing. Channel averaging effectively increases the bandwidth and consequently the rms noise in the average image will be smaller than that in the individual images. Smoothing of the image in the celestial plane effectively tapers the visibility in the (u, v)plane and consequently the effective number of visibility measurements is reduced. This implies that the beam-to-beam thermal fluctuations in the image will increase as the image is smoothed to lower resolutions. The effects of smoothing were determined by noting the fractional change in the peak of the 'dirty' beam (the resultant change in the sum of the weights of the visibility points) when the beam is convolved to resolutions corresponding to those of the four cubes, A through D.

No primary-beam correction was applied. This simplifies searches for the presence of signals above the noise level since the thermal-noise statistics will be uniform over the images. Positive detections, if any, will have to be subjected to a correction in flux density prior to interpretation. Upper limits derived from the data will therefore be relevant for an ‘effective’ search volume that is lower than the volume obtained from the observing bandwidth and the half power area of the primary beam.

In order to explore the existence of signals above the noise in the data cube, we have compared histograms of the pixel intensities with the distribution of intensities expected from thermal noise itself. We have chosen to compare the peak intensities with the predicted peaks based simply on Gaussian statistics. In a sample N independent measurements of a random variable obeying Gaussian statistics with a standard deviation of σ, the deviation x_m above which only one measurement is expected is given by the equation

$$\mathrm{erf}(x_m/\sqrt{2}\sigma) = (N-1)/N. \tag{6}$$

Table 1. A summary of the parameters of the four-smoothed spectral-line cubes.

Cube	Number of channel images	Resolution $\Delta\nu$ MHz	Resolution Δv km s^{-1}	Resolution $\Delta\theta$ arcsec	Comoving length d Mpc	M $M_\odot$/resol. element	Number of resol. elements per channel	x_m/σ per channel	Thermal rms noise mJy
A	12	0.244	244	70.6	1.42	4.6×10^{11}	1.7×10^4	4.0	3.1
B	6	0.488	488	141.3	2.84	3.7×10^{12}	4.2×10^3	3.7	4.1
C	4	0.732	672	211.9	4.25	1.2×10^3	1.9×10^3	3.5	4.6
D	2	0.976	895	282.5	5.67	3.0×10^{13}	1.0×10^3	3.3	5.0

Some images of the smoothed cubes had high intensity pixels which were confined to stripes at the image edges and are residuals from the interference-removal procedures adopted earlier in the analysis. After excluding these image edges, the final number of independent resolution elements per channel-image in each of the four cubes, as well as the expected values of x_m/σ for each channel-images as computed from equation (6), are also listed in Table 1. The noise statistics for the channel-images of the four cubes are listed in Table 2. We have displayed the histograms of the individual image pixel intensities in Fig. 2 for sample images from each of the four cubes. For each image, a grid of pixels spaced so as to roughly provide two pixels per resolution element have been used in creating the histogram. Parabolic profiles corresponding to Gaussian noise distribution have also been plotted as a reference. All the smoothed data cubes show no significant departures from Gaussian noise. For each image, we have compared the number of pixels (N_x) exceeding the value of x_m, which was computed using the rms values listed in Table 2, with the number of pixels per beam (N_b) for that image. This normalised ratio, N_x/N_b, is also listed in Table 2 for each image. Except for a couple of images in cube A, the ratio is in the range 0.4–2.3 as compared to the expected value of N_x/N_b = 1.0. This confirms the absence of significant systematic departures from Gaussian form in the tails of the distribution function.

Table 2. Statistics of the pixel-intensities in the images of the smoothed spectral-line cubes.

Cube	Image number	Freq. MHz	Max mJy	Min mJy	rms mJy	(N_x/N_b)
A	1	331.584	33.9	−29.8	7.0	2.0
	2	331.828	27.8	−25.1	5.2	2.3
	3	332.073	28.1	−26.0	5.0	5.0
	4	332.317	13.7	−12.7	2.9	2.0
	5	332.561	15.8	−16.7	3.5	1.7
	6	332.805	20.1	−19.6	3.8	2.3
	7	333.049	18.2	−17.5	3.9	2.0
	8	333.293	17.1	−16.7	4.0	0.3
	9	333.537	14.4	−14.3	3.3	2.0
	10	333.782	14.1	−17.7	3.0	2.5
	11	334.026	20.3	−22.5	4.2	3.6
	12	334.270	27.9	−26.6	5.9	1.2
B	1	331.706	38.0	−33.9	8.5	0.7
	2	332.195	25.2	−23.7	5.7	2.3
	3	332.683	23.1	−19.6	4.8	1.8
	4	333.171	21.0	−18.6	4.9	1.0
	5	333.569	15.3	−15.6	3.8	0.6
	6	334.148	29.3	−27.7	7.3	0.8
C	1	331.828	40.7	−49.0	11.5	0.6
	2	332.561	21.7	−49.0	11.5	1.0
	3	333.293	26.7	−22.8	6.1	0.9
	4	334.026	32.2	−32.8	8.1	0.4
D	1	332.536	22.1	−20.8	5.4	1.2
	2	333.513	22.5	−23.3	5.4	1.3

4. Interpretation of the data

The search covers a field 170.7 × 170.7 arcmin^2 which corresponds to an area of 206 × 206 h_{75}^{-2} Mpc^2 in comoving coordinates at z = 3.3. The survey bandwidth of 3.076 MHz corresponds to a depth of comoving length 17.9 h_{75}^{-1} Mpc. The resulting search volume is a rectangular parallelepiped having a comoving volume of 7.6 ×10^5 h_{75}^{-3} Mpc^3. The angular resolution of 70 × 57 arcsec^2, corresponding to the HPBW of the synthesised beam, implies a comoving linear resolution of 1.27 h_{75}^{-1} Mpc. The frequency resolution of 48.828 kHz implies a comoving linear resolution of 0.28 h_{75}^{-1} Mpc along the line-of-sight for matter having zero peculiar velocity with respect to the Hubble flow. The survey volume is expected to contain a total mass of 10^{17} $h_{75}^{-1} M_\odot$ assuming a mean matter density of closure value.

4.1 *Upper Limits on H I Density Fluctuations*

Considering the central channels in the four smoothed cubes, that are relatively interference free, there is no significant rms noise above that expected from the

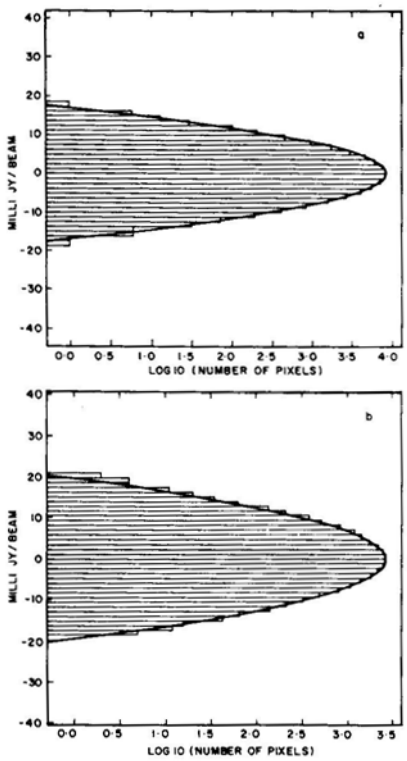

Figure 2. Histogram displays of the pixel intensities in selected images of the four smoothed cubes: 'a' pertains to channel 6 of Cube A; 'b' is for channel 4 of Cube B; 'c' is for channel 2 of Cube C; 'd' and 'e' are for channels 1 and 2 respectively of Cube D. In all the displays, continuous curves corresponding to Gaussian probability distribution functions are also plotted as a reference.

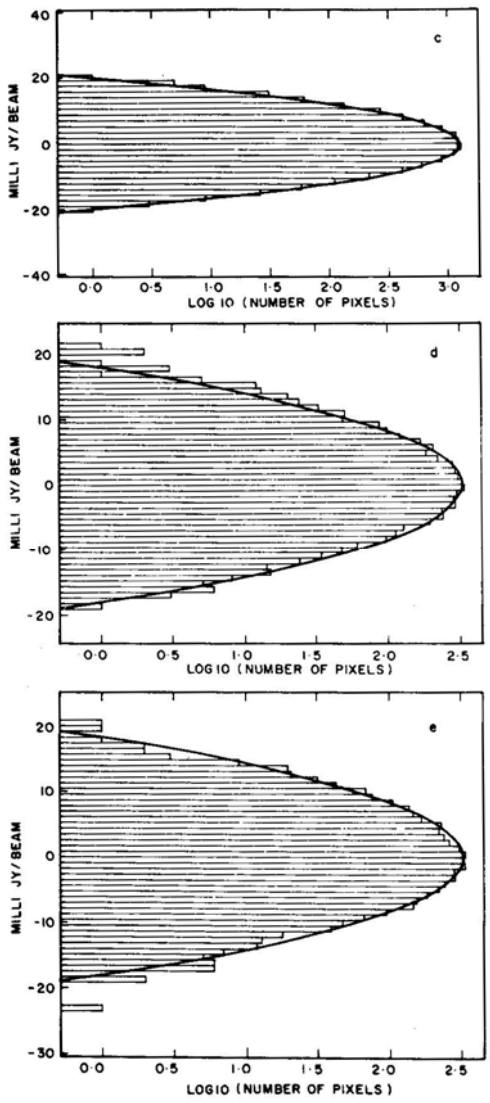

Figure 2. Continued.

instrument thermal noise. Hence we conclude that out experiment has not detected H I density fluctuations at redshift $z = 3.3$. Our results can nevertheless place upper limits on the rms H I density fluctuations at this redshift. Considering Cube D as an example, we note that the rms flux density is 5.4 mJy/beam, whereas the theoretically expected thermal noise is 5.0 mJy/beam. This implies a nominal excess fluctuation of 2.0 mJy/beam ($\approx \sqrt{(5.4)^2 - (5.0)^2}$). From the variations of the rms noise among the central 'good' channels within the four cubes, we judge that the error in our estimate of the mean observed rms is about 10 %. We also assume a 10 per cent error in our estimate of the standard deviation expected from thermal noise. Allowing for these errors, we obtain a 1σ limit of 4mJy/beam for the excess fluctuations in the flux density. Using Equation (5), this corresponds to a 1σ upper limit of $6 \times 10^{13}\, h_{75}^{-2}\, M_{\odot}$

for the H I density fluctuations. Assuming that baryonic matter, comprising of hydrogen and helium atoms in the number ratio 10:1, consitutes a fraction Ω_B of the mean matter density of the Einstein de Sitter Universe, these limits translate to a 1σ upper limit of $\Delta\rho/\rho$ of $3\Omega_B^{-1}$. We have summarised the results obtained using the central 'good' channels of all the four cubes in Table 3.

In order to comprehend the significance of these limits, we compare these with the $\Delta\rho/\rho$ of known astronomical objects. From the data in Lang (1980), we note that objects ranging from small groups of spirals to large groups of ellipticals possess a small spread in density around $6 \times 10^{13}\ M_\odot$ Mpc^{-3}. Assuming, as we have done above, that this represents the baryonic density which is a fraction Ω_B of the total closure density ($1.6 \times 10^{11}\ M_\odot$ Mpc^{-3}), these structures represent density enhancements of $\Delta\rho/\rho \approx 4000\Omega_B^{-1}$. If we adopt a value for Ω_B of 0.05, consistent with the constraints imposed by conventional theories of primordial nucleosynthesis (Yang *et al.* 1984), we find that groups of galaxies have a present day $\Delta\rho/\rho \approx 8000$. If the evolution of the parent perturbations are independent of the evolution on other scales, as is expected in a hierarchically developing universe, we infer from the discussions in Subrahmanyan (1990) that the parent perturbations of structures having the $\Delta\rho/\rho \approx 8000$ virialize at $z_v \approx 2.5$ and turn around at the redshift $z_m \approx 4.6$. Hence, at the redshift $z = 3.3$ their density contrast is expected to be ≈ 50. The low resolution cubes, C and D, that place constraints on H I density fluctuations on a proper length scale of $\sim 1 - 1.5$ Mpc at $z = 3.3$, are relevant for the derivation of constraints on the perturbations that are approaching the virialized state at $z = 3.3$ and which would lead to the formation of groups of galaxies having sizes ≈ 1 Mpc. From Table 3, we infer an upper limit of $\Delta\rho/\rho \approx 5/\Omega_B \approx 100$ (for $\Omega_B = 0.05$) on the H I mass fluctuations having the above scale at $z = 3.3$. The rms fluctuations permitted by the observational data are a factor of two larger than the intensity peaks expected if the progenitors of the present day groups of galaxies were neutral and gaseous at $z = 3.3$ It is interesting to note that by improving the sensitivity of the observations by a factor 4–6, which should be within the capabilities of future instruments like the Giant Metrewave Radio Telescope, it may be possible to directly observe the inhomogeneous matter distribution at high redshifts as fluctuations in intensity above the instrument thermal noise.

4.2 *Upper Limits on H I Masses of Condensates in the Search Volume*

We next turn our attention to the peak intensities observed at the various resolutions and derive firm upper limits on the H I masses of condensates within the search

Table 3. Upper limits on $\Delta\rho/\rho$ from limits on H I mass fluctuations.

Cube	Proper length scale Mpc	Expected thermal rms-noise mJy	Observed mean rms-noise mJy	Upper limit (1σ) on fluctuations due to H I inhomogeneities mJy	($h_{75}^{-2}\ M_\odot$)	1σ limits on $\Delta\rho/\rho$ (Ω_B^{-1})
A	0.33	3.1	3.5	2.7	1×10^{13}	< 30
B	0.66	4.1	4.5	3.3	2.5×10^{13}	< 9
C	1.00	4.6	5.6	4.6	5.3×10^{13}	< 6
D	1.32	5.0	5.4	3.9	6×10^{13}	< 3

Table 4. Upper limits on H I masses of condensates in the search volume.

Cube	Comoving search volume h_{75}^{-3} Mpc^3	Resolution element linear scale km s^{-1}	Mpc proper	$S_p\Delta v$ mJy MHz	M_{HI} h_{75}^{-2} $M_\odot$
A	85^3	224	0.33	4.9	0.77×10^{14}
B	84^3	448	0.66	11.3	1.8×10^{14}
C	83^3	672	1.00	19.5	3.0×10^{14}
D	74^3	895	1.32	22.7	3.5×10^{14}

volume. In cube D, over the entire comoving volume of (74 Mpc)^3, resolution elements having (5.7 Mpc)^3 volumes have an upper limit for $S_p\,\Delta v$ of 22.7 mJy MHz. Using Equation (5), this limit translates to an upper limit of $3.5 \times 10^{14}\ M_\odot$ for the mass of H I gas in any protocluster resident in the search volume. The corresponding limits derived from all the four smoothed spectral-line cubes are listed in Table 4. Structures in the present-day Universe ranging from small clusters of galaxies to rich clusters of galaxies possess virial velocities of several hundred km s^{-1} and H I masses in the range $10^{13} - 10^{15}\ M_\odot$, Their linear sizes range from a few hundred kpc to ≈ 1 Mpc. As seen from Table 4, our search covers the relevant range if we assume that the evolution of the virialised gaseous protoclusters to the present day rich clusters entailed only astrophysical processes with no dynamical evolution. The limits obtained in Table 4 do not place strong constraints on the lower mass clusters, but indicate that the richer clusters do not exist as gaseous condensates within our search volume at redshift $z = 3.3$.

4.3 *Implications for Abell Clusters*

The cores of rich clusters of galaxies represent the most massive virialized entities in the Universe today. We now examine our data seeking to detect the counterparts of these objects at the redshift $z = 3.3$. The cores have present day sizes ≈ 0.3 Mpc and masses of $\sim 10^{15}\ M_\odot$. The galaxies have a velocity dispersion $\approx 10^3$ km s^{-1}. These rich Abell clusters with richness class $R \geqslant 1$ have a comoving number density of $6 \times 1.0^{-6}\ h^3$ Mpc $^{-3}$ (Bahcall & Soniera 1983). For our adopted value of $h = 0.75$, we expect to find the counterpart of one such object in our (74 Mpc)^3 search volume. If these cluster cores have a constant proper dimension out to the redshift of $z = 3.3$, they should appear as emission features with a line width of ≈ 1 MHz and an angular size of ~ 1 arcmin. The central 40 channels of our spectral-line cube, at an angular resolution of ~ 1 arcmin and a frequency resolution of 1 MHz, display a peak intensity of 15 mJy/beam. The corresponding H I mass limit is $2.3 \times 10^{14}\ M_\odot$. Hence, neutral gaseous condensates corresponding to the present day rich Abell clusters are absent in our search volume although the counterpart of one rich Abell cluster is expected to be present. It is therefore possible that the rich Abell clusters did not exist as neutral gaseous condensates at $z = 3.3$.

4.4 *Implications for Protoclusters*

In this sub-section, all the matter at the search redshift is assumed to exist in the form of condensates (protoclusters) having a single arbitrary mass. These are not identified with known objects. The observational data is used to constrain their masses. In an Einstein-de Sitter universe, ~ 10 potentially observable condensates could exist in our search volume of 6×10^5 Mpc^3 if the individual condensate has a total mass of $\sim 10^{16}\ M_\odot$ For $\Omega_B = 0.05$, the H I mass within each condensate would be $\sim 4 \times 10^{14}\ M_\odot$ More than one of these objects are expected to be 'visible' if the lifetime of the condensate exceeds one tenth the dispersion in the epoch of their formation (which includes $z = 3.3$). The peak flux density detected within the survey region (Table 4) rules out the existence of condensates having the above H I mass within the search volume. Considering lower masses for the condensates, the assumptions stated above predict that greater than 10 'visible' condensates having H I masses of $\sim 4 \times 10^{13} M_\odot$ exist within the search volume. Considering the sensitivity achieved in our VLA observations, the existence of these condensates are ruled out only if their line-of-sight velocity dispersions do not exceed ~ 400 km s^{-1} . Hence, for the above assumptions in Ω_B and lifetimes, the VLA observations indicate that protoclusters with total masses $\sim 10^{16}\ M_\odot$ do not exist at $z = 3.3$ unless their velocity dispersions exceed $\sim 10^3$ kms $^{-1}$, with masses as low as $\sim 10^{15}\ M_\odot$ are unlikely unless their velocity dispersion exceeds ≈ 400 km s $^{-1}$ .The upper limit to the range of masses that are constrained is determined by the limited search volume and the lower limit is set by the search sensitivity. Increasing the assumed value for Ω_B or increasing the assumed lifetime would enable constraints on a greater range of masses. These VLA observations complement the observations in Subrahmanyan & Swarup (1990), where constraints were derived on larger mass condensates. As discussed in Subrahmanyan (1990), the velocity dispersion expected in a $10^{15}\ M_\odot$ scale over density at turn around is expected to be $\approx 10^3$ km s^{-1} for a smoothly peaked perturbation. Hence, the constraints derived here are valid even if the perturbations are yet to virialize.

5. **Comparison with earlier observations**

The observations of Hardy & Noreau (1987), that were also made using the VLA, covered a search volume that was a factor of 2.7 larger than the volume covered in our experiment. They adopted a channel-differencing technique for reducing the 'noise' level, with the consequence that only sources with velocity dispersions $\leqslant 350$ km s^{-1} would survive and a 2σ (2 standard deviation) upper limit of $3.6 \times 10^{14}\ h_{75}^{-2}\ M_\odot$ was inferred on the H I masses of protoclusters having this velocity dispersion Their comoving search volume of $1.5 \times 10^6\ h_{75}^{-3}$ Mpc^3 was located at a redshift $z = 3.3$. The observed rms-noise levels were a factor $\geqslant 5$ higher than the expected thermal noise and this was attributed to interference. The limits placed by their search were an order of magnitude poorer than our limits.

de Bruyn *et al.* (1988) used the WSRT to image a pair of fields at 327 MHz in spectral-line mode with a useful bandwidth of 2.0 MHz. The spectral-line cube was smoothed to various spatial and velocity resolutions in a matched-filter approach to

detect signatures of protoclusters. Since the flux density peaks in the smoothed cubes were as expected from thermal noise alone, upper limits in the range 3–13 $\times 10^{13}\ h_{75}^{-2}\ M_{\odot}$ were inferred on the H I masses of protoclusters that could exist in their search volume with a line-of-sight velocity dispersion in the range 150 to 1200 km s^{-1}. Their comoving search volume, encompassing $7 \times 10^5\ h_{75}^{-3}$ Mpc^3, was located at a redshift of $z = 3.3$. Our search volume was 85 % of the volume searched by de Bruyn *et al.* (1988) and our search sensitivity was a factor of two poorer.

The earlier workers derived upper limits to the masses of protoclusters that could exist in their search volume from the peak flux densities observed in their smoothed spectral-line cubes and this approach yields poorer limits if larger volumes were searched. Apart from computing limits in this manner, we have interpreted our data in certain novel ways. We have modelled the protoclusters as a population of condensates having an arbitrary but single mass, with reasonable assumptions for the H I content and lifetimes. The data have been interpreted as constraining the existence of protoclusters in dispersion velocity-mass space. The limits obtained would improve with increasing search volume. We have smoothed our independently observed data cube maintaining identical resolutions in all the three dimensions in comoving coordinates and hence derived upper limits on rms H I density fluctuations on a range of length scales. We have also specifically searched for counterparts of the present day Abell clusters at $z = 3.3$.

6. Conclusions

1. If the comoving space density of the protoclusters exceeds $(74\ Mpc)^{-3}$, condensates having $\geqslant 3.5 \times 10^{14}\ M_{\odot}$ in H I gas do not exist at the redshift of $z = 3.3$ in an Einstein-de Sitter universe. This result is valid provided that the line-of-sight velocity dispersion within the condensate is 1000 km s^{-1} Condensates having $\geqslant 5 \times 10^{13}\ M_{\odot}$ in H I gas are ruled out if their line-of-sight velocity dispersions are $\leqslant$ 400 km s^{-1} and their comoving space densities exceed $(35\ Mpc)^{-3}$.

2. Virialized neutral gaseous condensates, corresponding to the present day rich ($R \geqslant 1$) Abell clusters, are not present at the redshift of $z = 3.3$ if their comoving space densities exceed $(74\ Mpc)^{-3}$.

3. The VLA observations indicate an upper limit of $\approx 5\Omega_B^{-1}$ on the rms fractional density fluctuations at $z = 3.3$ on smoothing the matter distribution to a comoving linear scale of ~ 5 Mpc. This result is valid in an Einstein-de Sitter universe with Ω_B representing the mass fraction of the closure density that is in the form of neutral baryons.

The observations presented in Subrahmanyan & Swarup (1990) indicated that supercluster mass ($\geqslant 10^{15}\ M_{\odot}$ in H I gas) condensates do not exist at the redshift of $z = 3.3$. The observations discussed in this paper do not place strong constraints on supercluster scale structures, since less than 10 objects having H I masses $> 5 \times 10^{14}\ M_{\odot}$ are expected in the search volume for an adopted $\Omega_B \approx 0.05$. On the other hand, the VLA observations discussed in this paper indicate that protoclusters having H I masses in the range $4 \times 10^{13} - 4 \times 10^{14}\ M_{\odot}$ and having velocity dispersions ~ 400-1000 km s^{-1} may not exist in the neutral gaseous phase at the redshift of $z = 3.3$. This result suggests that counterparts of the groups and clusters of galaxies that we see in the present day Universe may not exist in the neutral gaseous phase at the

redshift z = 3.3. This implies that if condensates corresponding to the present day groups and clusters do form in the galaxy formation scenario, they are likely to have completed their gaseous phase prior to the redshift of z = 3.3. Since some of these structures that have low densities are expected to be still approaching the virialised state at that epoch, it appears that the groups and clusters do not form through a collapse of the parent gaseous perturbations followed by fragmentation into galaxies. The observations are suggestive of a scenario where galaxies form first followed by their clustering into groups and clusters as perturbations on larger scales turn around and undergo dissipationless collapse. Such a sequence of events is expected in a cold dark matter dominated universe. However, a neutrino dominated universe where the initial supercluster mass condensates fragment into galaxies at redshifts $z > 3.3$, followed by their undergoing hierarchical clustering, is not ruled out.

Acknowledgements

We thank Prof. Govind Swarup for his encouragement and helpful discussions. The NRAO is operated by Associated Universities, Inc., under cooperative agreement with the National Science Foundation. The data were reduced at the National Image Processing Facility for Astronomy (NIPFA) at the Radio Astronomy Centre, Ooty. This facility is financed by the Department of Science and Technology, Government of India. We also thank Juan Uson and Durga Bagri for useful discussions.

References

Bahcall, N. A., Soneira, R. M.1983, *Astrophys. J.,* **270**, 20.
Bebbington, D. H. O. 1986, *Mon. Not R. astr. Soc,* **218**, 577.
Bond, J. R., Szalay, A. S. 1983, *Astrophys. J.,* **274**, 443.
Clark, B. G. 1980, *Astr. Astrophys.,* **89**, 377.
De Bruyn, A. G., Wieringa, M. H., Katgert, P., Sancisi, R. 1988, in *IAU Symp. 132: Large Scale Structure of the Universe,* Eds Audouze, J., Pelletan M. C. & Szalay, A., D. Reidel, Dordrecht, p. 211.
Hogan, C. J., Rees, M. J. 1979, *Mon. Not. R. astr. Soc,* **188**, 791.
Hardy, E., Noreau, L.1987, *Astr. J.,* **94**, 1469.
Lang, K. R., 1980, *Astrophysical Formulae,* Springer-Verlag, Berlin, Heidelberg.
Napier, P. J., Thompson, A. R., Ekers, R. D. 1983, *Proc IEEE,* **71**, 1295.
Pearson, T. J. 1975, *Mon. Not. R. astr. Soc,* **171**, 475.
Pearson, T. J., Kus, A. J. 1978, *Mon. Not. R. astr. Soc,* **182**, 273.
Peebles, P. J. E., 1980, *Large Scale Structure of the Universe,* Princeton University Press, New Jersey.
Peebles, P. J. E., Yu, J. T. 1970, *Astrophys. J.,* **162**, 815.
Roelfsema, P. R. 1980, in *Proc Third NRAO Synthesis Imaging Summer School,* Eds Bridle, A., Schwab F. & Perley, R. A., *Astr. Soc. Of the Pacific Conference Series,* Vol. **6**.
Silk, J. 1968, *Astrophys. J.,* **151**, 459.
Subrahmanyan, R. 1990, *Mon. Not. R. astr. Soc,* Submitted.
Subrahmanyan, R., Swarup, G. 1990, J. Astrophys. Astr., submitted.
Sunyaev, R. A., Zel'dovich, Ya. B. 1974, *Mon. Not. R. astr. Soc,* **171**, 375.
Thompson, A. R.1982, *IEEE Trans. Antennas Propagat.,* **AP-30**, 450.
Thompson, A. R., Clark, B. G., Wade, C. M., Napier, P. J. 1980, *Astrophys. J. Suppl.,* **44**, 151.
Yang, J., Turner, M. S., Steigman, G, Schramm, D. N., Olive, K. A. 1984, *Astrophys. J.,* **281**, 493.